Renormalization group analysis of a quivering string model of posture control

Francisco Alonso-Sánchez[2,*] and David Hochberg[1,2,†]
[1]*Laboratorio de Astrofísica Espacial y Física Fundamental, Apartado 50727, 28080 Madrid, Spain*
[2]*Centro de Astrobiología (Associate Member of the NASA Astrobiology Institute), INTA, Carretera Ajalvir, Kilómetro 4, 28850 Torrejón de Ardoz, Madrid, Spain*
(Received 17 March 2000)

Scaling concepts and renormalization group methods are applied to a simple linear model of human posture control consisting of a trembling or quivering string subject to damping and restoring forces. The string is driven by uncorrelated white Gaussian noise, intended to model the corrections of the physiological control system. We find that adding a weak quadratic nonlinearity to the posture control model opens up a rich and complicated phase space (representing the dynamics) with various nontrivial fixed points and basins of attraction. The transition from diffusive to saturated regimes of the linear model is understood as a crossover phenomenon, and the robustness of the linear model with respect to weak nonlinearities is confirmed. Correlations in posture fluctuations are obtained in both time and space domains. There is an attractive fixed point identified with falling. The scaling of the correlations in the front-back displacement, which can be measured in the laboratory, is predicted for both large-separation (along the string) and long-time regimes of posture control.

PACS number(s): 87.10.+e, 05.10.Cc, 05.10.Gg, 05.70.Jk

I. INTRODUCTION

A wide variety of systems subject to noise, random forces, and interactions can be studied in depth by means of nonequilibrium statistical mechanics. This holds true whether the system in question is fundamentally of a chemical, biological, or physical nature. When the phenomena under study admits mathematical modeling by means of stochastic partial differential equations, many powerful techniques can be used to analyze the effects that noise, fluctuations, and random disturbances have on the dynamics as one changes both the spatial and temporal resolution scales at which the system is observed. The possibility to be able to use such techniques becomes especially pressing given that many typical real systems of interest are characterized by having many degrees of freedom interacting nonlinearly, leading to the competition between different length and time scales, with all scales evolving in the presence of noise and subject to uncontrollable external effects and contingencies. One of these important techniques is provided by the renormalization group, suitably extended to dynamical systems and systems out of equilibrium [1,2]. Some recent results of renormalization group analyses of the kind presented in this paper were obtained for diverse phenomena ranging from stirred fluids [3] and turbulence [4,5] to surface growth phenomena [6–10], flame front propagation [11], and cosmological large-scale structure formation [12–16].

Fluctuations and noise are known to be present in physiological systems as well. Recently, a simple continuum model of human posture control was proposed [17] that captures the gross or coarse-grained features underlying the physical mechanisms, and adjusts well to laboratory measurements of time-varying displacements of the front-to-back (anteroposterior) sway recorded for human subjects in an stationary upright stance [18,19]. Despite the fact that the actual human postural control system must undoubtedly be highly complex, the stochastic model introduced by Chow and Collins [17] is described by a linear, and hence, exactly solvable stochastic differential equation in one spatial dimension (in the following, temporal derivatives are denoted by an overdot, and the primes stand for spatial derivatives),

$$\beta\ddot{y}+\dot{y}-\nu y''+\alpha y=\eta(x,t), \tag{1}$$

where $y(x,t)$ denotes the time-dependent front-back displacement measured with respect to the vertical located at $y=0$ (here we take the x axis to denote the vertical axis, as z will be reserved for the dynamical exponent which we introduce and calculate below). This is of course immediately recognized as a one-dimensional wave equation subject to friction $(\dot{y})$, a linear restoring or pinning force (αy), and a stochastic or random force (η). The onset-of-damping time scale is set by β, the pinning time scale is set by α^{-1} and ν is an effective string tension parameter. (This continuum equation describes the motion of a quivering damped string with a linear restoring force. A discrete version of this model would involve a chain of coupled random walkers, or monomers, and in this guise can be denoted as a pinned polymer [17]). The stochastic noise is taken to be Gaussian with zero mean. For subsequent calculational purposes, it is convenient to characterize the noise spectrum directly in Fourier space (k,ω),

$$\begin{aligned}\langle\eta(k,\omega)\rangle&=0,\\ \langle\eta(k,\omega)\,\eta(k',\omega')\rangle&=\Gamma(k,\omega)(2\pi)^2\delta(k+k')\,\delta(\omega+\omega'),\end{aligned} \tag{2}$$

where the angular brackets denote averaging with respect to the noise, and the noise spectrum function $\Gamma(k,\omega)$ may in general contain both short and long range correlations in space and/or time. We consider white noise here, so the spec-

*Electronic address: alonso@laeff.esa.es
†Electronic address: hochberg@laeff.esa.es

tral function is proportional to a constant noise amplitude: $\Gamma = 2\mathcal{A}$ In Ref. [17], noise exhibiting short-time temporal correlations but uncorrelated (or white) for long-time scales was used in computing the correlation and response functions directly from the Fourier transform of the wave equation [Eq. (1)], where the former were fit to laboratory posture data allowing a phenomenological determination of β and α^{-1}, an effective noise amplitude, and a parameter characterizing the short-time noise correlations.

In Ref. [17] it was claimed that nonlinearities are not necessary to explain the posture data of healthy standing individuals, though it was also recognized that this may not be the case for subjects with balance disorders (nor even for normal individuals subject to a sufficiently large perturbing ''kick''). These effects clearly lie outside the scope of the linear model [Eq. (1)], as do posture displacements outside the sway envelope or cone of stability [20,21], and there is clear motivation for extending that model to include weak nonlinear terms. The minimal nonlinear term one can include in Eq. (1) is of the form $\sim y^2$, which also serves to break the $y \to -y$ symmetry in Eq. (1). Including this quadratic term makes good sense from the physiological point of view, since real anteroposterior motion is intrinsically asymmetric [17]. Physically, this amounts to having a ''pinning force'' that varies with the amplitude of the horizontal displacement y. We will see, moreover, that such a term is needed in order to account for falling. In this paper we analyze the importance and impact of weak nonlinearities and to check the robustness of the linear model by means of a dynamical renormalization group (RG) analysis. We therefore consider a nonlinear stochastic wave equation given by

$$\beta\ddot{y} + \dot{y} - \nu y'' + \alpha y + \epsilon y^2 = \eta(x,t), \tag{3}$$

where $\epsilon \geqslant 0$ is the strength of the quadratic nonlinearity, and we take the noise spectrum to be white (i.e., uncorrelated) at large scales: that is, $\Gamma(k,\omega) = 2\mathcal{A}$, where the noise amplitude is denoted by $\mathcal{A}$, which also serves as a loop-counting parameter [22] [an expansion of the solutions of Eq. (3) in loop diagrams is a convenient and powerful way to organize the calculation].

We are interested in the correlations in the solution(s) of Eq. (3) in the so-called hydrodynamic limit corresponding to large spatial separations (along the vertical axis) and long-time intervals: $|x - x'| \to \infty$ and $|t - t'| \to \infty$. This will tell us how the posture fluctuations are correlated along the length of the body at any given instant, and how they are correlated in time at any given point on the body. In terms of Fourier variables (momentum k and frequency ω), this limit is taken by letting $(k,\omega) \to 0$. The scaling information and universality class of this nonlinear wave equation is contained in two critical exponents: the dynamic exponent z and the ''roughness'' exponent χ. These exponents are first obtained via a simple scale transformation of the stochastic equation of motion, and forms part of the full RG transformation (a course graining or thinning out of the degrees of freedom, followed by a rescaling) [1]. A change of space and time scales $x \to sx$, $t \to s^z t$ is accompanied by a corresponding change of scale in the displacement field variable $y \to s^\chi y$. Under this scaling the stochastic equation of motion Eq. (3) transforms according to

$$s^{-z}\beta\ddot{y} + \dot{y} - s^{z-2}\nu y'' + s^z \alpha y + s^{z+\chi}\epsilon y^2 = s^{(1/2)(z-1)-\chi}\eta, \tag{4}$$

where we have used the noise two-point correlation function [Eq. (2)] to determine the scaling of the noise source. Under this transformation, the individual parameters appearing in Eq. (3) therefore scale as

$$\begin{aligned} \beta &\to s^{-z}\beta, \\ \nu &\to s^{z-2}\nu, \\ \alpha &\to s^z \alpha, \\ \epsilon &\to s^{z+\chi}\epsilon, \\ \mathcal{A} &\to s^{z-2\chi-1}\mathcal{A}. \end{aligned} \tag{5}$$

At a *fixed point* of this scaling, the model parameters and the field y no longer change under a rescaling for certain specific values of the exponents z and χ. The model parameters approach their fixed-point values $\beta \to \beta^*$, $\nu \to \nu^*$, etc., and this fact gives rise to a corresponding fixed-point equation of motion, which is Eq. (3) written in terms of the fixed-point parameters. Thus each fixed point corresponds to a distinct dynamics governing the long time and large distance ($s \to \infty$) behavior of the model. The dynamical phase space is thus divided or ''partioned'' into various domains or basins of attraction (or repulsion), each domain associated with a given fixed point. We can use this fixed point information to predict the asymptotic scaling of the displacement correlation function in both the temporal and spatial domains. This will be one of the main objectives of this paper.

Independently of the RG, and in preparation for the results to be obtained, it is useful to derive the general scaling form of the correlation function of transverse displacements. Under a global scale transformation, the displacement field transforms according to

$$y(sx, s^z t) = s^\chi y'(x,t), \tag{6}$$

which merely states that under a space and time rescaling, the displacement field can, and generally does, transform into a distinct (hence the prime) functional form y', apart from picking up an overall factor. Thus a change of scale will generally change the function itself, *unless* one is in the scaling or power law regime. When the system is known to be in a scaling regime, then in fact $y = y'$ and from Eq. (6), the autocorrelation function therefore scales as

$$\begin{aligned} \langle y(x,t)y(0,0)\rangle &= s^{-2\chi}\langle y(sx,s^z t)y(0,0)\rangle, \\ &= x^{2\chi}\Psi\left(\frac{t}{x^z}\right), \end{aligned} \tag{7}$$

where (without loss of generality) we have chosen $s \sim x^{-1}$, and Ψ is a (dynamic) scaling function, which itself exhibits a power law behavior for asymptotic limits of its argument:

$$\Psi(u) = \begin{cases} A & \text{for } u \to 0 \\ Bu^{2\chi/z} & \text{for } u \to \infty, \end{cases} \tag{8}$$

for constants A and B. The dynamic exponent z describes the scaling of relaxation times with length and χ is the ''roughness'' exponent of the string or polymer. Thus a knowledge of these two exponents is all that is required to determine the explicit scaling of the correlation function within each dynamic phase of the model. For the linear model (i.e., $\epsilon=0$) these exponents can be exactly determined with little effort, and there are just two solutions (for white noise). For one, the wave equation for nonvanishing pinning force ($\alpha\neq 0$) is made scale invariant with the choices $z=0$ and $\chi=-\frac{1}{2}$. This exponent solution can be read directly from Eq. (5), taking into account the fact that the noise amplitude is constant and hence, nonvanishing on all scales ($\mathcal{A}>0$). This immediately yields the exponent identity $z=2\chi+1$. For a finite fixed value of the pinning force, the only possibility is to take $z=0$, since a positive $z>0$ yields an asymptotically divergent α, while $z<0$ would instead yield an asymptotically vanishing value. We see that $\beta^*=\beta$ is finite and the diffusion constant vanishes, $\nu^*=0$. In this phase, then, there is no diffusion. This exponent pair corresponds to the experimentally observed scaling regime denoted as ''bounded'' or ''saturated,'' and holds for the very latest times when the pinning force has had time to correct for posture excursions from the vertical and aligns the body in an upright stance [17]. In the earlier ''diffusive'' scaling regime, the pinning force did not have sufficient time to act and is negligible, i.e., $\alpha\approx 0$, and there is another exact exponent solution given by $z=2$ and $\chi=\frac{1}{2}$, indicating that in this parameter regime, the model belongs to the same universality class as the one-dimensional Edwards-Wilkinson model [25]. At this fixed point, we have a finite diffusion $\nu^*=\nu$ and $\beta^*=0$. In this phase, there is no wave propagation, since the second derivative in time is absent. Note that these simple scaling solutions have been obtained from applying naive scaling arguments to the *linear* equation. However, as soon as the nonlinearity ϵ is turned on, and no matter how weak, other nontrivial exponent solutions arise for which the nonlinearity can become *relevant*. The naive scaling arguments are insufficient for obtaining the scaling exponents in the fully nonlinear model. The RG allows one to calculate z and χ in the combined presence of fluctuations and nonlinearities, and to calculate the exact asymptotic scaling of the correlation function [Eq. (7)] in all the basins of attraction.

The rest of this paper is organized as follows. In Sec. II we make use of a dynamic functional formalism for the perturbative calculation of solutions to Eq. (3) based on the Martin-Siggia-Rose Lagrangian. The bare correlation function, response function, noise spectral function, and bare interaction vertex function are identified; their corresponding Feynman diagrams are also introduced and calculated, and these provide the basic elements of a systematic and controlled loop expansion for the one-particle-irreducible diagrams which we then use for extracting the one-loop RG equations in the low-energy regime.

In Sec. III we exhibit a set of nonlinear differential RG equations for the dimensionful parameters appearing in Eq. (3). For white noise these involve five equations: one associated with each independent parameter appearing in the equation of motion. We then identify a convenient set of three dimensionless couplings in terms of which these RG equations can be expressed. The RG flow is therefore represented in a three-dimensional dimensionless parameter space, and we solve for all the one-loop fixed points in terms of this reduced set. In this way we find a total of two trivial fixed lines and four nontrivial fixed points. Linearization of the RG about each fixed point (or line) reveals the *nature* of the fixed point, in the dynamical systems sense (whether the fixed point is a source, a sink, a limit cycle, a spiral, a saddle point, etc.) and yields linear stability information which we quote in terms of the eigenvalues and eigenvectors of the linearized RG. The two lines of fixed points correspond to the diffusive and bounded phases of the strictly linear model, and are present in the nonlinear model for all values of α and β. Of the four nontrivial fixed points, one is a stable spiral which represents the ''falling'' phase. The other three are saddle points which seem to have rather little influence on the long-range and long-time dynamics, however.

Substitution of the fixed points back into the original set of RG's yields the values of the critical exponents z and χ for each fixed point, and hence determines the exact asymptotic scaling properties of the correlations [Eq. (7)] in the basin of attraction (or repulsion) of each fixed point, which is presented in Sec. IV. The numerical analysis of the fixed points is then repeated using an alternative set of three dimensionless parameters suitable for investigating the small α limit (corresponding to the diffusive regime). The use of this second set of parameters in conjunction with the first is necessary in order to completely cover the entire model parameter space.

The detailed structure of the nonlinear RG flow is revealed by plotting the fixed points and mapping the numerically computed (and normalized) vector field of the nonlinear RG flow in the neighborhoods of all the points in Sec. V. Many important aspects of the morphology of the dynamic phase space are qualitatively revealed, and allow conclusions to be drawn regarding the impact of the weak nonlinearity. This provides revealing information regarding the shape and structure of the basins of attraction, and complements the analytic analysis. Summary and conclusions are drawn in Sec. VI.

A number of explicit analytic calculational details needed for the derivation of the RG equations are relegated to the Appendixes. The complete calculations leading to the one-loop response function are presented in Appendix A, and similar calculations for the noise spectral function and vertex renormalizations are given in Appendixes B and C, respectively.

II. DYNAMIC FUNCTIONAL FORMALISM

In this section we make use of a functional integral representation of non-equilibrium stochastic dynamics. This leads to the efficient identification and extraction of the calculational elements (and Feynman rules) needed for the perturbative calculation of the solutions of any stochastic partial differential equation. It is well known how to map stochastic ordinary or partial differential equations with additive noise into equivalent generating functionals [24,23]. Essentially, there are two formally distinct but physically equivalent routes one may follow, an option one has at least in the case of Gaussian noise. In the Martin-Siggia-Rose (MSR) formalism [26–28] one introduces a fictitious conjugate field (call it

$\hat{y}$) with its own source term. The equation of motion, in this case given by Eq. (3), is imposed as a constraint on the dynamic functional, and is realized linearly. In the minimal formalism, no conjugate field is introduced, leading to a nonlinear realization of the constraint [23,22]. For Gaussian noise in the minimal formalism, the constraint appears quadratically in the argument of the functional, while for non-Gaussian noise it inherits whatever nonlinearities are present in the noise probability distribution function itself [22]. Here we develop a calculation following the MSR approach, since this leads to a simpler structure for the associated Feynman diagrams, and our immediate aim is to obtain a perturbation expansion which can be set up, organized, and calculated in terms of a few elementary diagrams or graphs.

The MSR dynamic generating functional corresponding to Eq. (3) is given by (taking a translationally invariant noise spectrum)

$$Z[J,\hat{J}]=\int [dy][d\hat{y}]\exp\Bigg(-\frac{1}{2}\int dxdt\,\hat{y}\Gamma\hat{y} + i\int dxdt\,\hat{y}\{\beta\ddot{y}+\dot{y}-\nu y''+\alpha y+\epsilon y^2\} + \int dxdt(yJ+\hat{y}\hat{J})\Bigg), \tag{9}$$

where $\hat{y}$ denotes the conjugate field, and J and $\hat{J}$ are arbitrary sources for y and $\hat{y}$, respectively. The noise η has been integrated out exactly, and appears in this functional only through its two-point or correlation function Γ. There is also in principle a certain Jacobian determinant factor in passing from Eq. (3) to Eq. (9), but it can be shown on general grounds to be a constant, and hence irrelevant for computing normalized correlation functions (see, e.g., Refs. [23,22]). The noise spectrum Γ as written here is understood to be given in terms of x and t. All the dynamic and fluctuation information contained in Eq. (3) is also contained in Z, which is an alternative representation of the dynamics. In preparation for the RG transformation, which is most straightforwardly implemented in the Fourier domain, we cast this functional in terms of momentum and frequency variables from the outset.

To this end, we introduce Fourier transforms for the physical and conjugate fields and the noise spectrum, i.e.,

$$y(x,t)=\int^{>}\frac{dk}{2\pi}\int_{-\infty}^{\infty}\frac{d\omega}{2\pi}y(k,\omega)e^{i(kx-\omega t)}, \tag{10}$$

where, in a mild abuse of notation, we distinguish the functions from their Fourier transforms only through their arguments; this, however, avoids a clutter of notation later on. Note that we implicitly cut off the momentum integration at the scale $\Lambda=2\pi/a$, where a plays the role of a minimum distance of spatial resolution or lattice spacing. The cutoff symbol on the integral ($>$) means one is to integrate over all momenta in a ''shell'' such that $\Lambda/s<|k|<\Lambda$ where $s>1$ [see Eq. (A6)]. The cutoff defines the spatial scale above which it makes sense to use continuum equations for modeling. The quadratic or Gaussian part of the functional (i.e., $\epsilon=0$) can be exactly computed, and serves as the starting point for a perturbative expansion which we will use to calculate the RGE equations associated with the nonlinear stochastic wave equation [Eq. (3)]. From standard Gaussian integrations [24,23], we have that (up to an overall irrelevant constant prefactor)

$$Z_0[J,\hat{J}]=\exp\Bigg(\int^{>}\frac{dk}{2\pi}\int_{-\infty}^{\infty}\frac{d\omega}{2\pi} \times\Bigg\{\frac{\frac{1}{2}J(k,\omega)\Gamma(-k,-\omega)J(-k,-\omega)}{\omega^2+[\nu k^2-\beta\omega^2+\alpha]^2} + i\frac{\hat{J}(k,\omega)J(-k,-\omega)}{i\omega-\beta\omega^2+\nu k^2+\alpha}\Bigg\}\Bigg). \tag{11}$$

From Eq. (9), it is clear that all noise averages of arbitrary products of physical fields and conjugate fields at distinct points and times are obtained from the appropriate functional derivatives of $\ln(Z)$ with respect to the source terms J and $\hat{J}$, taking the sources to zero at the end of the calculation. We may thus obtain the ''bare'' or zeroth order autocorrelation and response functions directly in Fourier space [the zero (0) subscript denotes the zero-coupling limit $\epsilon=0$] as

$$\begin{aligned}\langle y(p_1,\omega_1)y(p_2,\omega_2)\rangle_0 &= \frac{(2\pi)^4}{Z_0[J,\hat{J}]}\frac{\delta^2 Z_0[J,\hat{J}]}{\delta J(p_1,\omega_1)\delta J(p_2,\omega_2)}\Bigg|_{J=\hat{J}=0}\\ &=(2\pi)^2\delta(p_1+p_2)\delta(\omega_1+\omega_2)\frac{\Gamma(p_1,\omega_1)}{\omega_1^2+[\nu p_1^2-\beta\omega_1^2+\alpha]^2}\\ &\equiv(2\pi)^2\delta(p_1+p_2)\delta(\omega_1+\omega_2)C(p_1,\omega_1),\end{aligned} \tag{12}$$

for the autocorrelation function, and

$$\begin{aligned}\langle y(p_1,\omega_1)\hat{y}(p_2,\omega_2)\rangle_0 &= \frac{(2\pi)^4}{Z_0[J,\hat{J}]}\frac{\delta^2 Z_0[J,\hat{J}]}{\delta J(p_1,\omega_1)\delta\hat{J}(p_2,\omega_2)}\Bigg|_{J=\hat{J}=0}\\ &=i\frac{(2\pi)^2\delta(p_1+p_2)\delta(\omega_1+\omega_2)}{i\omega_1-\beta\omega_1^2+\nu p_1^2+\alpha}\\ &\equiv(2\pi)^2\delta(p_1+p_2)\delta(\omega_1+\omega_2)i\Delta(p_1,\omega_1),\end{aligned} \tag{13}$$

for the response function. The final equations in each case define the corresponding *reduced* autocorrelation and response function C and Δ, respectively. The δ function factors reflect the fact that momentum and energy (or frequency) are conserved as they ''flow'' through the correlation and response functions. It will be noted that the reduced response and correlation functions are related via $C=\Delta^*\Gamma\Delta=\Gamma|\Delta|^2$, and this relation will be used to obtain the noise amplitude renormalization from knowledge of the correlation function. They also automatically satisfy the fluctuation-dissipation theorem: $C(p,\omega)=(\Gamma/\omega)\mathrm{Im}\,\Delta(p,-\omega)$. The re-

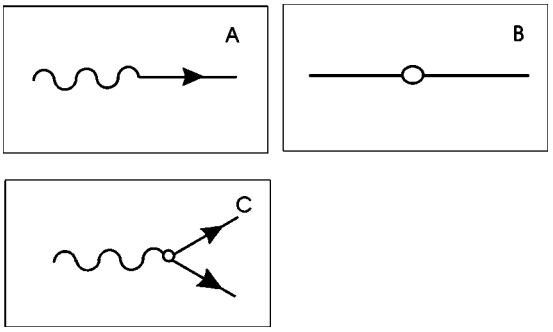

FIG. 1. (A): The bare response function. (B) The bare correlation function. (C) The bare vertex function.

maining element from which the complete perturbative expansion of the dynamic functional is developed is provided by the vertex function, which necessarily involves the trilinear interaction term. The complete dynamic functional [Eq. (9)] can be written as

$$Z[J,\hat{J}]=\exp\left(S_I\left[\frac{\delta}{\delta J},\frac{\delta}{\delta\hat{J}}\right]\right)Z_0[J,\hat{J}]=\sum_{n=0}^{\infty}\frac{(S_I)^n}{n!}Z_0[J,\hat{J}], \tag{14}$$

where the exponential of the following interaction operator acts on the Gaussian part (Z_0) of the generating functional,

$$S_I\left[\frac{\delta}{\delta J},\frac{\delta}{\delta\hat{J}}\right]=i\epsilon\int\left\{\prod_{j=1}^{3}\frac{dk_j d\omega_j}{(2\pi)^2}\right\}(2\pi)^2\delta(k_1+k_2+k_3)\times\delta(\omega_1+\omega_2+\omega_3)(2\pi)^6\times\frac{\delta^3}{\delta\hat{J}(k_1,\omega_1)\delta J(k_2,\omega_2)\delta J(k_3,\omega_3)}, \tag{15}$$

and merely reflects the fact that the nonlinear interaction term for the MSR functional is a *cubic* interaction involving one conjugate field and two factors of the physical field: $\sim i\epsilon\hat{y}y^2$. The δ functions are a consequence of the energy and momentum conservation at the vertex, and the strength of the vertex is given by the parameter ϵ, which in fact defines the reduced vertex. We complete the specification of the elements encountered in a perturbative expansion of Z by specifying the vertex function, which we read off simply by inspection of Eq. (15):

$$\epsilon(k_1,k_2,k_3;\omega_1,\omega_2,\omega_3)=(2\pi)^2\delta(k_1+k_2+k_3)\delta(\omega_1+\omega_2+\omega_3)i\epsilon. \tag{16}$$

Each of these calculational elements C, Δ, Γ, and ϵ, can be represented by a simple diagram as depicted in Fig. 1, and then used to systematically construct a perturbation expansion of the dynamic functional, and its Legendre transform

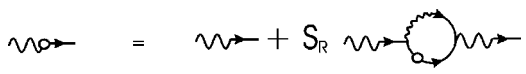

FIG. 2. The one-loop corrected response function.

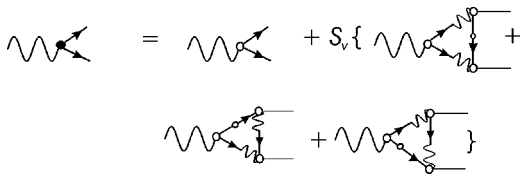

FIG. 3. The one-loop corrected vertex function.

(or effective action) which is the generator of the one-particle irreducible (1PI) diagrams. [Note that we remove the factor of i appearing in the bare vertex (15) and response functions (13) by redefining the conjugate field $\hat{y}\rightarrow i\hat{y}$ in the functional integral.] The Feynman diagram for the bare response function Δ is shown in Fig. 1(A), which reflects the fact that the response function is constructed from the mixed product of the conjugate field (wiggly line segment) times the physical field (straight line segment). The arrow indicates the direction in which momentum k and frequency ω flow through this diagram (from the conjugate to the physical field), and is the convention we adopt here. It is important to keep this in mind since $\Delta(k,\omega)\neq\Delta(-k,-\omega)$, as can be seen by inspection of Eq. (13). The bare correlation function is shown in Fig. 1(B). As this is an even function in both momentum and frequency, we need not indicate a flow direction for this function. Finally, the bare trilinear vertex is shown in Fig. 1(C). This involves one conjugate field and two physical fields. The bare interaction is represented by a small open circle. The arrows indicate the flow direction for the two physical fields and is just a convention; the crucial point is that momentum and frequency are conserved at each vertex, as per Eq. (16). These are used to build up the 1PI diagrams, which are those diagrams that cannot be broken down into disconnected subdiagrams by cutting an internal line (see examples below). The class of 1PI diagrams are of fundamental importance in any perturbative scheme based on diagrams since all other diagrams can be unambiguously built up from these primitive ''building blocks.'' In Figs. 2–4 we depict the 1PI one-loop diagrams contributing to the noise spectrum, response function and vertex function. These diagrams are built up from the elementary vertex and response and correlation functions. Note that the bare correlation function is itself a *composite* function built up from the noise spectrum and response functions and is *not* 1PI. This fact is also reflected mathematically in the fact that the bare correlation, noise, and response functions obey a fluctuation-dissipation theorem. The complete mathematical transcription of the diagrams is carried out in the Appendixes.

Finally, we note that each loop diagram is multiplied by an overall symmetry factor. This factor receives a contribution from the factorial coming from expanding out the exponential prefactor in Eq. (14) to a given order in the coupling. For example, a graph with n bare interaction vertices yields a factor of $1/n!$. The other contribution comes from simply counting the number of distinct ways in which the given diagram can be built out of elementary Feynman graphs [Figs. 1(A)–1(C)], keeping the topological structure fixed [29]. Multiplying these two numbers together yields the final

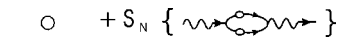

FIG. 4. The one-loop corrected noise spectral function.

net symmetry factor. For the response, noise, and vertex one-loop diagrams, these turn out to be $S_R=4$, $S_N=2$, and $S_V=4$, respectively.

III. DYNAMIC RENORMALIZATION GROUP EQUATIONS AND THEIR FIXED POINTS

By means of a diagrammatic expansion, we calculate the one-loop corrections to the response function Δ, the noise spectral function Γ, and the nonlinear vertex ϵ, and from these we obtain the associated one-loop corrections to the model parameters α, β, ν, $\mathcal{A}$, and ϵ in the large-distance and long-time limits. The complete one-loop expressions are derived and calculated explicitly in Appendixes A, B, and C for the response function, noise spectral function, and interaction vertex, respectively. With these in hand, the next task is to carry out the renormalization group transformation, leading to the differential flow equations, whose steps we briefly review here [1].

(1) We first perform an infinitesimal Kadanoff or ''block'' transformation: that is, we integrate over a thin momentum shell $\Lambda/e^l \leqslant |k| \leqslant \Lambda$, where $l=1+\delta$, $0<\delta \ll 1$. This means we integrate over (small-scale) fluctuations characterized by having their momentum in the range $(\int_{-\Lambda}^{-\Lambda/e^l} + \int_{\Lambda/e^l}^{\Lambda})(dk/2\pi)$. Physically, this step serves to thin out the degrees of freedom (coarse graining), and reduces the spatial resolution of the system. Note that in one space dimension, the ''momentum shell'' reduces to two disjoint intervals. For $d \geqslant 2$ and higher, it is a thin spherical shell in momentum space.

(2) After performing this step, the resulting equations have a new, lower momentum cutoff of Λ/e^l. This means we have changed the lattice constant of the system, this, to restore it to its original size, we rescale the momenta by putting $k \to k e^{-l}$. This is identical to the scaling carried out earlier with $s=e^l$. The parameters are rescaled (but here, differentially) as in Eq. (5), but with additional corrections coming from the momentum-shell integrations carried out in step (1).

Applying these steps to the one-loop expressions (A8), (B5), and (C4), we obtain the following set of differential renormalization group flow equations,

$$\frac{d\alpha}{dl} = \alpha\left(z - \frac{2g}{(1+h)^2}\right),$$

$$\frac{d\beta}{dl} = \beta\left(-z - \frac{g}{(1+h)^2}\left\{f + \frac{1}{2f(1+h)^2}\right\}\right),$$

$$\frac{d\mathcal{A}}{dl} = \mathcal{A}\left(z - 2\chi - 1 + \frac{4g}{4f(1+h)-1} \times\left\{\frac{f^2}{(1+h)} + \frac{3f}{4(1+h)^2} - \frac{1}{4(1+h)^3}\right\}\right), \quad (17)$$

$$\frac{d\epsilon}{dl} = \epsilon\left(z + \chi + \frac{2g}{(1+h)^2}\left\{\frac{1}{(1+h)} - f + \frac{1}{4f(1+h)-1} \times\left[4f^2(1+h) + 3f - \frac{1}{(1+h)}\right]\right\}\right),$$

$$\frac{d\nu}{dl} = \nu\left(z - 2 + \frac{2g}{4f(1+h)-1}\left\{\left[2 - \frac{8hf}{4f(1+h)-1}\right] \times\left(-\frac{f^2}{(1+h)} + \frac{5f}{4(1+h)^2} - \frac{1}{4(1+h)^3}\right) + 4h\left(\frac{3f^2}{2(1+h)^2} - \frac{f}{(1+h)^3} + \frac{1}{4(1+h)^4}\right)\right\}\right),$$

where the three *dimensionless* parameters g, h, and f are defined by

$$g = \frac{\epsilon^2 \mathcal{A}\Lambda}{\pi\alpha^3}, \quad h = \frac{\nu\Lambda^2}{\alpha}, \quad f = \alpha\beta. \quad (18)$$

This reduction from five dimensionful to three dimensionless parameters is a concrete realization of a more general result from dimensional analysis known as Buckingham's Π theorem [30], which states that if one has m dimensionful variables in a theory involving n fundamental units (such as length, time, mass, etc.) then there exist $m-n$ independent dimensionless groups or combinations of the m original quantities. In our case, $m=5$ and $n=2$, since all the parameters appearing in the stochastic equation (3) can be expressed in terms of two fundamental units: namely length and time. Thus we expect to be able to write the five RG equations exclusively in terms of $5-2=3$ independent dimensionless groups or combinations of the original dimensionful parameters. The fact that a cutoff is introduced from the RG transformation presents no problem since $|\Lambda| = L^{-1}$ has units of inverse length. The number of fundamental units remains the same. Below we introduce a second, independent group of three dimensionless parameters which when taken with this first set, will suffice to *cover* the entire parameter space.

The dimensionless coupling controlling the nonlinearity is g, and a nonzero value of this coupling is what drives the RG flow away from the free, or Gaussian, limit. Since $g \propto \epsilon^2 \mathcal{A}$, to have a nontrivial flow simultaneously requires both a nonvanishing nonlinearity $\epsilon \neq 0$ *and* fluctuations $\mathcal{A} > 0$. Indeed, by setting $g=0$ in Eq. (17), we immediately recover the naive scaling laws given by Eq. (5), expressed here in differential form, with $s=e^l$. Thus we see that the model parameters depend on scale in a complicated way when nonlinearities ($g \neq 0$) are present. In terms of these dimensionless variables, the RG flow is given by the following set of three differential equations:

$$\frac{dg}{dl} = g\left(-1 + \frac{g}{(1+h)^3}[15 + f(1+h) + 6h]\right),$$

$$\frac{dh}{dl} = h\left(-2 + \frac{g}{(1+h)^4}[3 + 3h + 2h^2 + f(-1 + 2h + 3h^2)]\right), \quad (19)$$

$$\frac{df}{dl} = -\frac{g}{2(1+h)^4}[1 + 4f(1+h)^2 + 2f^2(1+h)^2].$$

These are obtained by differentiating Eq. (18) and using Eq. (17). Note that the dependence on the two exponents has dropped out. We solve for the complete set of real fixed

TABLE I. Fixed points in terms of g, f, and h.

Fixed Point	Position $(g*,h*,f*)$	Critical exponents (z,χ)	IR eigenvalues	IR eigenvectors	Class
$L1$	$(0,0,f)$	$(0,-1/2)$	$(-2,-1,0)$	$v_{L1}^1=(1,0,0)$ $v_{L1}^2=(0,1,0)$	Stable line attractor
$P2$	$(-0.37,-2.15,-1.79)$	$(-0.56,-0.41)$	$(-6.79,-0.67\pm0.27i)$	$v_{P2}^1=(-0.17,-0.99,0.03)$ $v_{P2}^2=(0.57+0.11i,0.72,-0.24-0.28i)$ $v_{p2}^3=(0.57-0.11i,0.72,-0.24+0.28i)$	Stable spiral
$P3$	$(0.07,0,-0.29)$	$(0.14,-0.41)$	$(-1.78,1,-0.10)$	$v_{P3}^1=(0.06,1.00,-0.04)$ $v_{P3}^2=(1.00,0.00,0.00)$ $v_{P3}^3=(0.00,0.00,1.00)$	Saddle point
$P4$	$(0.08,0,-1.71)$	$(0.15,-0.45)$	$(-1.65,1.,0.11)$	$v_{P4}^1=(0.08,1.00,-0.04)$ $v_{P4}^2=(1.00,0.00,0.00)$ $v_{P4}^3=(-0.01,0.00,1.00)$	Saddle point
$P5$	$(2.86,-2.96,-0.07)$	$(1.48,0.03)$	$(-8.24,1.50,-1.28)$	$v_{P5}^1=(0.21,0.98,0.01)$ $v_{P5}^2=(0.97,-0.23,0.01)$ $v_{P5}^3=(0.79,0.45,-0.41)$	Saddle point

points whose coordinates are (g^*,h^*,f^*). These are labeled, collected, and presented in Table I along with their associated critical exponents, infrared eigenvalues, and eigenvectors, and the nature of the fixed point. There is actually an entire line of attractive fixed points, denoted by $L1$, located at $(0,\ 0,\ f)$, where f is any real number. A fit of the linear model to the data yields $f^*=0.05$. As we will see, $L1$ is associated with the final saturated phase for which $\nu^*=0$. This implies that $h^*=0$. In the linear model $g=g^*=0$, so the posture data picks out a distinguished point on the line $L1$, and we see the final phase of posture control is controlled by an infrared attractive fixed point at $(0,0,f^*)$. The quadratic term gives rise to three saddle points $P3$, $P4$, and $P5$, and one stable spiral $P2$; their coordinates are listed in the second column of Table I. When we substitute these fixed points into the original set of RG equations (17), we obtain the corresponding pair of critical exponents: $z=z(g^*,h^*,f^*)$, $\chi=\chi(g^*,h^*,f^*)$ associated with each fixed point (or fixed line),

$$z=\frac{2g^*}{(1+h^*)^2},$$
$$\chi=\frac{(1-g^*[3+f^*(1+h^*)+2h^*]+h^*[3+3h^*+h^{*2}])}{2(1+h^*)^3}, \tag{20}$$

which we obtain from using the pair of equations for $\mathcal{A}$ and α in Eqs. (17) to solve for z and χ. Any pair of equations depending on z and χ taken from Eqs. (17) can be used to solve for these exponents, provided that neither equation in the pair *trivially* evaluates to zero at the fixed point whose exponents one wishes to compute (thus, for example, if $\beta^*=0$; then we cannot use the equation $d\beta/dl=0$ to solve for z, and so forth.). Taking this obvious restriction into account, we have checked that the exponents calculated taking all possible pairs of the RG equations agree. This serves as an important consistency check of the entire calculation. The exponents are listed in the third column of Table I. By linearizing the RG equations (19) around each fixed point, we obtain additional information regarding the stability of the fixed point and can classify the infrared stability properties of the point. This information is helpful for visualizing the RG flow and interpreting the flow graphs in Sec. V. At each fixed point we substitute $g=g^*+\delta g$, $h=h^*+\delta h$, $f=f^*+\delta f$, into Eqs. (19) retain all terms up to order $O(\delta g,\delta h,\delta f)$, and compute the eigenvectors and eigenvalues of this linear system. This information completely characterizes the RG flow in the linearized neighborhood of each fixed point. The eigenvalues and eigenvectors are listed in columns four and five of Table I. The unit direction vectors in this coupling space have components $\hat{g}=(1,0,0)$, $\hat{h}=(0,1,0)$, and $\hat{f}=(0,0,1)$. Note that the line $L1$ has only two RG flow eigenvectors associated with it. From knowledge of the eigenvalues, we immediately predict the nature of the fixed point, and this is given in the last column of Table I.

Of the four nontrivial fixed points, three of them $(P2,P3,P4)$ are well within the limits of perturbation theory, as they all correspond to small values of the dimensionless coupling $|g^*|<1$. By contrast, the coupling for the $P5$ fixed point turns out to be rather large: $g^*=2.86>1$, and it is likely this point is an artifact of perturbation theory. In any event, as can be seen from inspection of the graphs in Sec. V, $P5$ is ''far'' away from the remaining fixed points, and has very little or no impact on the RG flow in the small coupling region, which is the region safely explored by perturbation theory. Both $P3$ and $P4$ are near the point $(0,0,f^*)$ belonging to $L1$, but a study of the flow in the neighborhood of $(0,0,f^*)$ shows these to be unimportant, and substantiates the claim made in Ref. [17] that nonlinear effects are not needed to explain posture data of *healthy* individuals. Nevertheless, nonlinearities are needed to account for falling, and the stable spiral $P2$ is an attractor for ''falling,'' as we now show. For $P2$ the fixed coupling $g^*=-0.37$ is *negative*. But $g^*<0\Rightarrow\alpha^*<0$, since $\epsilon^2>0$ and $\mathcal{A}>0$, and a change in sign of α signals the transition from stability of the upright vertical stance $y=0$ to instability or falling: $y>0$. This can be seen quite clearly by examining the properties of the effec-

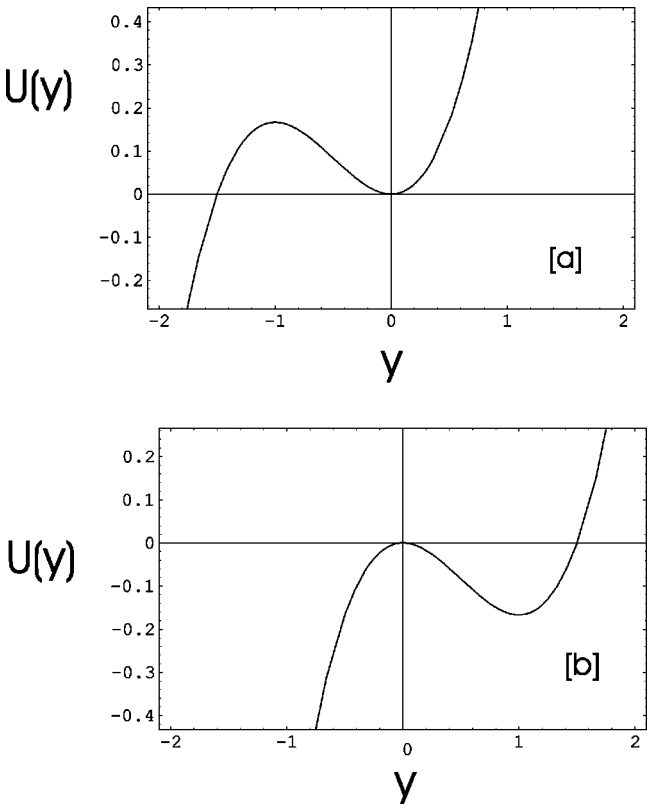

FIG. 5. Effective mechanical potential $U(y)$ for (a) $\alpha>0$ and (b) $\alpha<0$. $U(y)$ has units of energy, and y has units of length.

tive mechanical potential $U(y)$ associated with our equation. This potential is obtained by integrating the y-dependent force terms appearing in Eq. (3) and yields

$$U(y)=\tfrac{1}{2}\,\alpha y^2+\tfrac{1}{3}\,\epsilon y^3, \tag{21}$$

since $F(y)=-U'(y)$ is the deterministic (non-random) force acting on the string. A plot of U versus y is shown for $\alpha>0$ and for $\alpha<0$ in Fig. 5, where $U(y)$ is plotted along the vertical and y along the horizontal axes, respectively.

For $\alpha>0$, the origin at $y=0$ is locally stable to small perturbations (to fall, one would have to be pushed backwards sufficiently hard so as to overcome the potential barrier at $y=-1$. However, when $\alpha<0$, the vertical stance becomes an unstable configuration, and a fall in either direction results (a clear mechanical example of symmetry breaking). This falling phenomena is beyond the scope of the linear model since α is always positive in the linear model. The flow graphs in Sec. V reveal that $P2$ lies in a domain or phase which is separated from the domain or phase of upright stance. Thus, healthy individuals are characterized by having their initial conditions of posture control the basin of attraction of $L1$.

The above group of dimensionless couplings forms a useful set when ν is small, and the limit as ν tends to zero (corresponding to vanishing viscosity or diffusion) can be safely studied. The limit of small β can also be treated with this set. When α is small, however, corresponding to the diffusive regime, a different set of couplings is required. To study the flow corresponding to $\alpha\to 0$ (corresponding to a vanishing linear restoring force), we introduce the set of dimensionless variables

$$G=g/h^3=\frac{\epsilon^2\mathcal{A}}{\pi\nu^3\Lambda^5},\quad H=h^{-1}=\frac{\alpha}{\nu\Lambda^2},\quad F=f=\alpha\beta. \tag{22}$$

In terms of these new variables, the original set of RG flow equations (17) takes the following forms:

$$\frac{d\alpha}{dl}=\alpha\left(z-\frac{2G}{H(1+H)^2}\right),$$

$$\frac{d\beta}{dl}=\beta\left(-z-\frac{G}{(1+H)^2}\left\{\frac{F}{H}+\frac{H}{2F(1+H)^2}\right\}\right),$$

$$\frac{d\mathcal{A}}{dl}=\mathcal{A}\left(z-2\chi-1+\frac{G}{(1+H)^2}\left\{\frac{F}{H}+\frac{1}{(1+H)}\right\}\right), \tag{23}$$

$$\frac{d\nu}{dl}=\nu\left(z-2+\frac{G}{(1+H)^4}\left\{H-1+\frac{F}{H}(3+2H-H^2)\right\}\right),$$

$$\frac{d\epsilon}{dl}=\epsilon\left(z+\chi+\frac{4G}{(1+H)^3}\right).$$

By setting $G=0$, we once again recover the naive scaling laws given by Eq. (5). In terms of this group of three dimensionless couplings, the RG equation flow is characterized by

$$\frac{dG}{dl}=G\left(5+\frac{G}{H(1+H)^4}[4F(-2-H+H^2)+6H(2+H)]\right),$$

$$\frac{dH}{dl}=2H+\frac{G}{(1+H)^4}[-2-3H-3H^2+F(-3-2H+H^2)], \tag{24}$$

$$\frac{dF}{dl}=F\left(-\frac{GH}{2F(1+H)^4}-\frac{2G}{H(1+H)^2}-\frac{FG}{H(1+H)^2}\right).$$

These result from differentiating Eq. (22) and using Eq. (23). Once again, the dependence on the two exponents z and χ drop out of the equations for the dimensionless variables. We solve for the complete set of real fixed points, which we denote collectively by (G^*,H^*,F^*) and are displayed in the second column of Table II. We note that we reproduce two of the fixed points obtained with the original variables, namely, $P2$ and $P5$. Although their coordinates as expressed with the variables (G,H,F) are distinct from those in the (g,h,f) system, their exponents, eigenvalues, and eigenvectors are identical in both systems. Once again, we see that $P2$ is an attractor for falling: in these variables $G^*>0\Rightarrow\nu^*>0$ so that $H^*<0\Rightarrow\alpha^*<0$.

We also discover a repulsive fixed line 11 located at $(0,0,F)=(0,0,f)$. This fixed line was ''missed'' by the first group of parameters. The posture data in the diffusive phase selects a point on this line, namely, (0,0,0.05).

We substitute these fixed points into the original set of RG equations (23) to obtain the corresponding pair of critical exponents: $z=z(G^*,H^*,F^*)$, $\chi=\chi(G^*,H^*,F^*)$ at each fixed point:

TABLE II. Fixed points in terms of G, F, and H.

Fixed point	Position $(G*,H*,F*)$	Critical exponents (z,χ)	IR eigenvalues	IR eigenvectors	Class
11	$(0,0,F)$	(2,1/2)	(5,2,0)	$V^1_{L1}=(1,0,0)$ $V^2_{L1}=(0,1,0)$	Unstable line
$P2$	$(0.04,-0.46,-1.79)$	$(-0.56,-0.41)$	$(-6.79,-0.67\pm0.27i)$	$V^1_{P2}=(0.16,-0.98,-0.13)$ $V^2_{P2}=(0.05-0.02i,0.25-0.30i,0.92)$ $V^3_{P2}=(0.05+0.02i,0.25+0.30i,0.92)$	Stable spiral
$P5$	$(-0.11,-0.34,-0.07)$	(1.48,0.03)	$(-8.24,1.50,-1.28)$	$V^1_{P5}=(-0.72,-0.69,0.09)$ $V^2_{P5}=(-0.39,0.88,0.26)$ $V^3_{P5}=(0.19,0.12,0.97)$	Saddle point

$$z=\frac{2G^*}{H^*(1+H^*)^2},\quad \chi=-\frac{2G^*(1+3H^*)}{H^*(1+H^*)^3}. \tag{25}$$

These follow from taking the equations for ϵ and α. Taking other pairs of RG equations yields expressions for the exponents that evaluate to the same numerical values at the fixed points. In analogy with the first set of RG equations, we calculate the eigenvalues and eigenvectors associated with the linearization of Eqs. (24) about each fixed point (fixed line), and determine the nature of each point from the eigenvalues. This information is organized in Table II.

IV. CORRELATION FUNCTION: SCALING PROPERTIES

As discussed in Sec. I, the RG fixed-point analysis can be used for predicting the asymptotic, large-distance, and long-time limits of the two-point correlation function of transverse displacements from the vertical upright position,

$$C(x_1-x_2,t_1-t_2)=\langle[y(x_1,t_1)-y(x_2,t_2)]^2\rangle, \tag{26}$$

which measures the fluctuations in the difference of transverse displacements at two different points along the body and/or at two different times. Because the model is translationally invariant, this function depends only on the differences x_1-x_2 and t_1-t_2 in space and in time. In the scaling regime, which holds when the system is in the vicinity of one of its fixed points, it is easy to derive the exact scaling behavior of Eq. (26) which emerges in the large-distance and long-time limits. Put $x=x_1-x_2$ and $\tau=t_1-t_2$. Consider correlations in a time domain measured at the same point on the body, so that $x=0$. Then from $y(x,\tau)=s^{-\chi}y(sx,s^z\tau)$ we have that

$$C(0,\tau)=s^{-2\chi}C(0,s^z\tau)\sim\tau^{2\chi/z}C(0,1)=B\tau^{2\chi/z}, \tag{27}$$

with B a constant, which follows from choosing s such that $s^z\tau=1$. Next, for correlations in the spatial domain, we set $\tau=0$ and obtain

$$C(x,0)=s^{-2\chi}C(sx,0)\sim x^{2\chi}C(1,0)=Ax^{2\chi}, \tag{28}$$

which follows from choosing s such that $sx=1$; A is a constant. These results are consistent with and imply the scaling limits of the scaling function Ψ appearing above in Eq. (7).

Using Tables I and II, it is a simple matter to calculate the scaling of the correlation function about each fixed point. First, we consider the limiting case represented by ''turning'' off the quadratic interaction term: $\epsilon\to0$. In this limit, we recover the linear model of Chow and Collins [Eq. (1)], and we reproduce the corresponding scaling behavior(s) of the correlation function. In this limit (and for uncorrelated noise) there are then only the two trivial fixed points (actually, fixed lines) $l1$ and $L1$ (see Table I), corresponding to the small α and small ν limits, respectively. Reading off the critical exponents from Table I and using Eq. (27), we confirm that in the neighborhood of $l1$ the correlation function scales as $C(\tau)=B\tau^{1/2}$. [In Ref. [17] the temporal correlations are parametrized as $C(\tau)\sim\tau^{2H}$, so this corresponds in our notation to $H=1/4$, since evidently, $2H=1/2$.] This exponent $2H=1/2$ falls well within the experimental range of 0.52 ± 0.12, which is exactly equivalent to the exponent $H=1/4$ falling within the experimental range 0.26 ± 0.06 which is the one cited in Ref. [17]. In the neighborhood of $L1$, we see that $z=0$, indicating the relaxation time is independent of length scale and is indicative of a saturated regime. Care must be taken in calculating the correlation function, since the resulting exponent in Eq. (27) is formally divergent. If we write the correlation function (26) in terms of the auto-correlation function $C(\tau)=2[S(0)-S(\tau)]$, and use the scaling of the latter as derived in Eq. (7), we see that $S(\tau)\sim\lim_{z\to0}\tau^{-1/z}=0$, so that $C(\tau)\to2S(0)\sim\tau^0=\text{const}$. This reproduces the scaling obtained by Chow and Collins by other means. Unfortunately, the error in the null exponent for the saturated regime is unknown. These two power laws correspond to the two scaling regions termed ''diffusive'' and ''saturated,'' respectively. Note, moreover, that $l1$ is repulsive, and therefore unstable to the slightest perturbation (fluctuation), while $L1$ is stable and attractive. These lines lie within a common two-dimensional RG flow domain (in the $h-f$ plane), and the transition from diffusive to saturated behavior is understood from the RG point of view as a crossover phenomenon; see Fig. 6. This plot shows $l1$ to be at a finite distance in h above $L1$. The RG flow as determined from the linear model starts from a point on $l1$, and drops vertically until it ends up on $L1$. The locus of all possible flows ''starting'' from points on $l1$ forms a ''curtain'' which is depicted in this figure. We superpose the complicated RG flow due to the nonlinear interaction for sake of comparison. Actually, while $g^*=G^*=0$ is consistent with zero coupling $\epsilon=0$, and $f^*=F^*$ holds simultaneously, there is in fact an inverse (and singular) relation between h and H, namely, $H=1/h$. Since $L1$ has $h^*=0$, the other line $l1$, when plotted in terms of these coordinates (g,h,f), is actually infinitely far away from $L1$. We

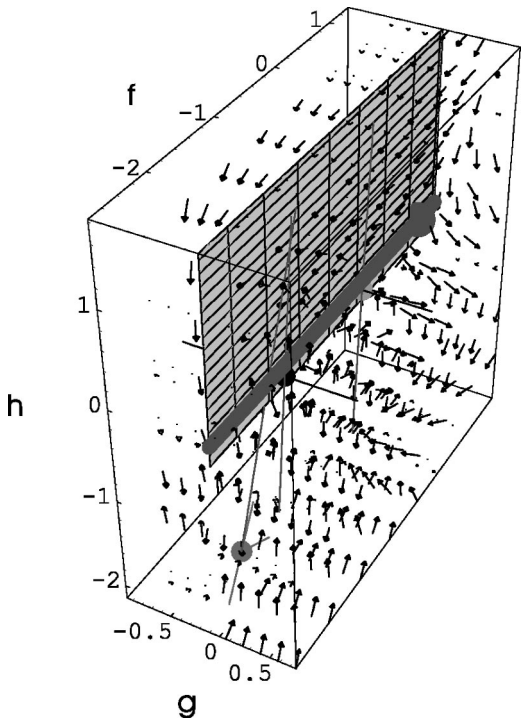

FIG. 6. Renormalization group flow between $l1$ and $L1$ in the $h-f$ plane.

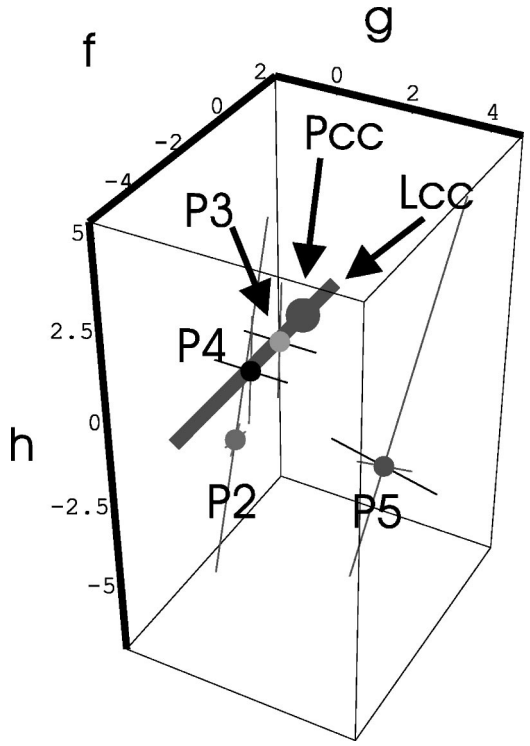

FIG. 7. The fixed line $L1$, experimental point P_{CC}, and $P2-P5$. The plotted eigenvectors are taken from Table I.

interpret this as an artifact of the model, which, remember, is based on an *infinitely* long string. Thus, for an infinitely long body, the transition to the saturated or bounded phase would never take place (the crossover time would be infinite). But this makes perfect physical sense since in fact saturation is a finite-size effect. This connection between a finite system size and saturation is also drawn for phenomena in surface growth phenomena [10]. Real bodies are of course finite in size, and these two fixed lines would be separated by a finite distance in h.

This crossover time scale is given by α^{-1}, and a fit to the data yields $\alpha^{-1}\approx 10$ sec [17]. Restoring the nonlinear term $\epsilon>0$ gives rise to an additional nontrivial structure in RG parameter space. In total we have the two trivial fixed lines ($l1$,$L1$) plus the four nontrivial fixed points: $P2$, $P3$, $P4$, and $P5$. The scaling behavior of the correlation function in both the time and space domains is listed below in Table III.

The scaling of $C(\tau)$ associated with the trivial fixed lines $l1$ and $L1$ reproduces that obtained previously in Ref. [17], where the (bare) correlation function was calculated directly in the linear model. The behavior of $C(\tau)$ in the vicinity of the nontrivial fixed points $P2$, $P3$, $P4$, and $P5$ is due entirely to the presence of the nonlinear term $\sim y^2$ in the equation of motion. The scaling behavior in the *spatial* fluctuations encoded in $C(x)$ was not discussed in Ref. [17], but these can be computed just as easily as the temporal fluctuations and are listed in the third column of Table III for completeness. These together with the behavior of $C(\tau)$ for the nontrivial fixed points constitute predictions of the (nonlinear) model within all the phases. We draw particular attention to the scaling of the correlation function in the vicinity of the stable spiral $P2$, which as we demonstrated in Sec. I is an attractor for falling.

TABLE III. Scaling behavior of the correlation function about each fixed point.

Fixed Point	$C(\tau)=B\tau^{2\chi/z}$	$C(x)=Ax^{2\chi}$
11	$\tau^{1/2}$	x^{1}
$L1$	τ^{0}	x^{-1}
$P2$	$\tau^{1.5}$	$x^{-0.8}$
$P3$	$\tau^{-5.9}$	$x^{-0.8}$
$P4$	$\tau^{-6.0}$	$x^{-0.9}$
$P5$	$\tau^{0.04}$	$x^{0.1}$

V. RENORMALIZATION GROUP FLOW

The two-dimensional RG flow for the strictly linear model (Fig. 6) is rather featureless and uniform, and lends itself to easy interpretation. Although we have depicted it in the two-dimensional coupling plane $h-f$, as already pointed out, the phenomenology of posture control picks out a single point on each of the fixed lines $l1$ and $L1$, (0,0,F^*) and (0,0,f^*), respectively, and the RG flow is actually a one-dimensional line. In marked contrast, the RG flow for the nonlinear model fills out the full three-dimensional coupling space (g,h,f). The relative locations of $L1$, $P2$, $P3$, $P4$, and $P5$ are shown in Fig. 7, where we have suppressed the flow for better visibility. The largest point on the heavy line $L1$ represents the experimentally determined point $P_{CC}=(0,0,0.05)$, and one can appreciate the close proximity of the two saddle points $P3$ and $P4$ in the neighborhood of this point. The stable spiral $P2$ is further away and the other saddle point $P5$ is furthest removed from $L1$. The actual numerical coordinates of all these objects are listed in Table I. We have found that the RG flow is best represented in terms of the (normalized)

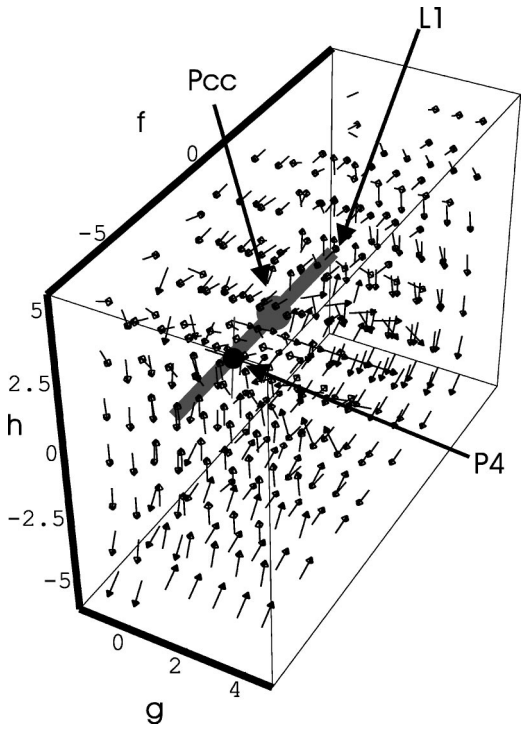

FIG. 8. The RG flow in the vicinity of *CC* and *P*4.

instantaneous direction field, obtained from directly plotting the differential equations (19) as functions of (g,h,f). In normalizing, we lose information about the instantaneous ''speed'' of the flow, but retain a sense of flow direction and flow morphology. The instantaneous magnitudes of the flow vectors changes abruptly and dramatically, and, without normalization, makes the graphs extremely difficult to plot. We plot each fixed point with its local system of numerically determined eigenvectors. The lengths and directions of each eigenvector system is taken from Table I. The remaining graphs represent a selection of direction flow fields calculated in the vicinity of the fixed points, for various ranges of the coupling *g*, where the complicated nature of the RG flow can be best appreciated.

The structure of the RG flow is shown in Fig. 8, which gives a ''close-up'' view of the flow in the vicinity of the experimental point and the saddle point *P*4. Gross features can be appreciated, such as the circulation coming from the region of positive *f* and a sudden change of the flow in the region of negative *f*, which we interpret as signaling the presence of a phase boundary or domain. In the closer vicinity of the fixed points the flow is attracted to the point *CC*. Since *P*4 is a saddle point, the flow does not end up there, but is ''deflected'' when it passes by.

In Fig. 9, we show the structure of the RG flow in the vicinity of *CC* and the stable spiral *P*2.

In Fig. 10, we view the same flow field as before, but drawing the points *P*3 and *P*4 in their respective positions. Figure 11. gives the same view, but with an extended range of the coupling *g*, while in Fig. 12 the range in *g* is extended even further and only the points P_{CC} and *P*3 are drawn in place (also see Fig. 13).

VI. SUMMARY AND DISCUSSION

We have extended Chow and Collin's linear pinned-polymer model of posture control by including a weak quadratic nonlinearity. There are at least two good reasons for doing this. First, in real anteroposterior movement, the front-to-back sway is not symmetric with respect to the vertical upright position. An obvious way to account for this fact is

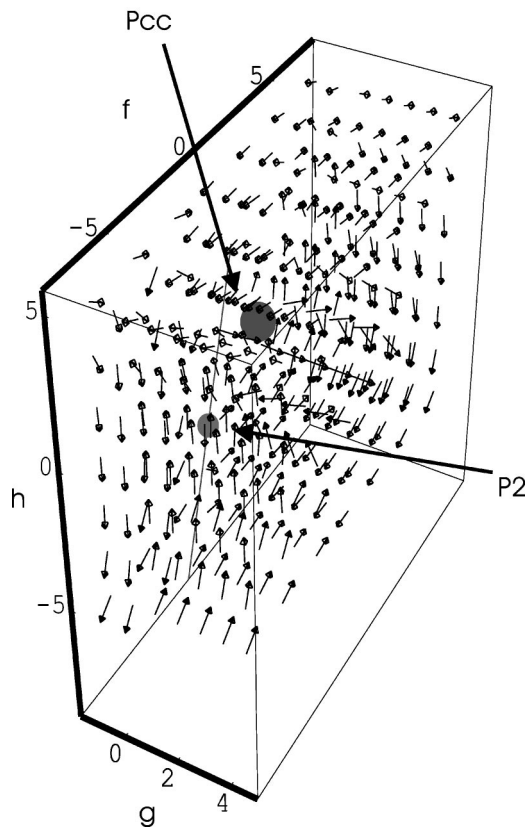

FIG. 9. The RG flow in the vicinity of *CC* and the stable spiral *P*2.

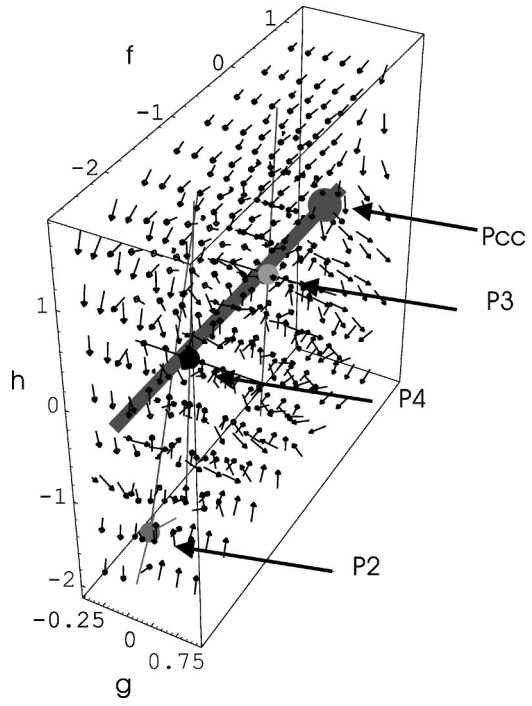

FIG. 10. The RG flow in the neighborhood of *CC*, *P*3, *P*4, and *P*2.

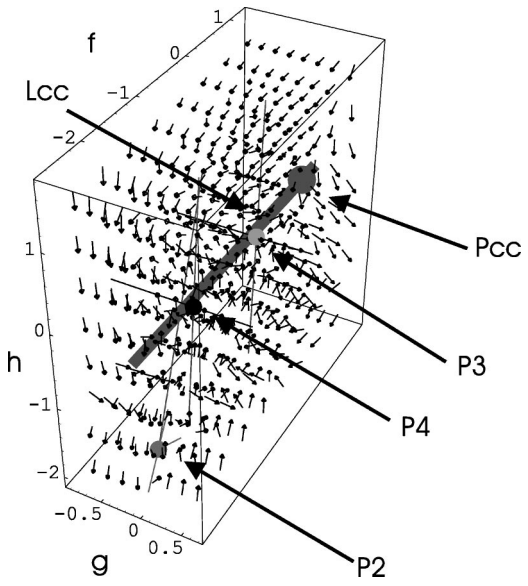

FIG. 11. The RG flow in the neighborhood of *CC*, *P*3, *P*4, and *P*2.

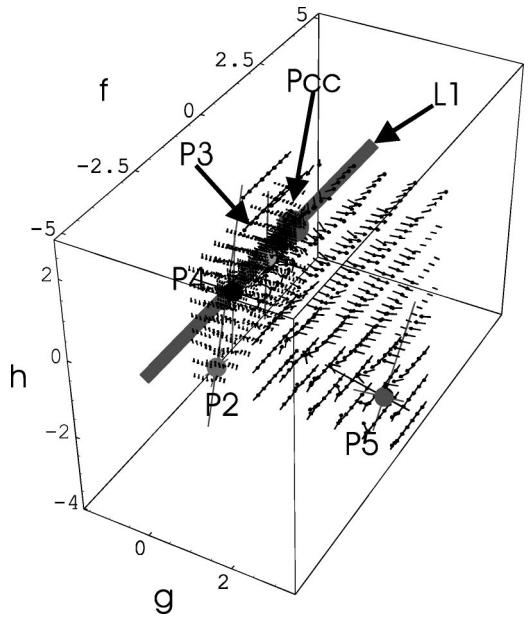

FIG. 13. All points and the flow field are included.

to introduce a symmetry-breaking term in the polymer equation of motion, and a minimal term that can be added is second order or quadratic in the displacement field y. Second, effects such as stepping or falling are beyond the scope of the linear model, and these can be approximately modeled by means of nonlinear terms in the equation of motion [31]. The analysis of nonlinear equations is a complicated enterprise, but the techniques afforded by the renormalization group permit one to obtain a wealth of information regarding the dynamical phases of the system for both large-distance and long-time limits. We have undertaken a detailed RG analysis of the fully nonlinear model, and summarized our results in terms of RG fixed points, stability analysis, and exponents. We have also numerically computed the fully nonlinear RG flow, and represented this in terms of a normalized vector flow field. Knowledge of the RG fixed points is sufficient for determining the exact power-law behavior of the correlation function of posture displacement in both temporal and spatial domains. In the linear limit of the model we recover the diffusive and saturated phases of posture control, and compute the scaling of the correlation function within each phase. The transition from the diffusive phase to the saturated phase, and the associated change in the scaling exponent are, crossover phenomena. However the crossover time is finite only for finite-size systems, as we have argued. These results agree with the linear analysis of Chow and Collins [17]. The quadratic nonlinearity gives rise to four nontrivial fixed points. There are two saddle points near the attractive trivial fixed point. While they do alter the RG flow in the neighborhood of the trivial attractive fixed point, they have no bearing on either of the two linear phases (diffusive and saturated) of the model. The linear model fits the posture data rather well, and the detailed analysis undertaken here substantiates the claim made in Ref. [17] that weak nonlinearities are not needed to explain the posture data of healthy individuals.

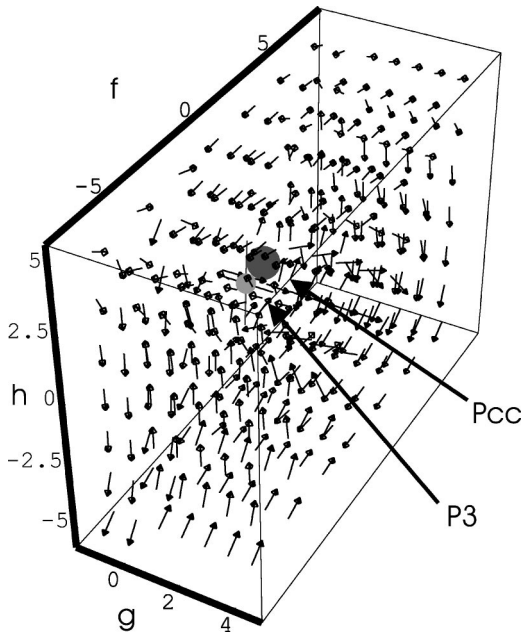

FIG. 12. The RG flow in the neighborhood of *CC* and *P*3.

The other two nontrivial fixed points consist of an additional saddle point and a stable spiral. The saddle point corresponds to a large value of the dimensionless coupling constant, and is probably an artifact of perturbation theory. Much more interesting is the spiral, which is purely attractive and, as we have shown, is associated with a falling phase. Its domain of attraction appears to be separated from the diffusive and saturated domains. It is important to note that the quadratic nonlinearity is the minimum term that can be added to the equation of motion that serves to *break* the anteroposterior symmetry. This symmetry breaking has lead to a falling phase, and thus this one term simultaneously fulfils two distinct requirements. In Ref. [31], falling was modeled with a nonlinear potential, but the nonlinearity employed there does not break the $y \rightarrow -y$ symmetry.

Mention should be made of the short-time inertial effects which are not covered in the present analysis, and which are

important for an understanding of posture control. These seem to imply the existence of short-time correlations in the noise [17], and it is therefore no surprise that the purely white uncorrelated noise used here is unable to reproduce this early scaling regime. Nevertheless, the analysis carried out here can be straightforwardly extended to handle both white and colored noise, and some comments to this effect are provided in Appendix D. Although our analysis has centered on the application to posture control, variants of stochastic differential equations of the type considered here have applications to a host of other problems where nonlinear waves propagate in a noisy and/or random medium [32], and the general details of the RG analysis carried out here should be useful for addressing these other applications.

ACKNOWLEDGMENTS

We thank David R. C. Domínguez for many interesting discussions during the early stages of this work, and for supplying us with independent numerical integrations of the differential RG equations. This work was financed in part by INTA, FSE (Fondo Social Europeo), FEDER, CSIC (Consejo Superior de Investigaciones Superiores), CAM (Comunidad Autónoma de Madrid) and OCYT (Oficina de Ciencia y Tecnología de la Presidencia del Gobierno).

APPENDIX A: RESPONSE FUNCTION: ONE-LOOP CORRECTION

The explicit analytic expression for the one-loop correction (hereafter denoted by primes) to the response function (13) follows immediately from transcribing the diagrammatic representation of the corrected response function (see Fig. 2) into its corresponding mathematical elements

$$\begin{aligned}\Delta'(p,\omega)&=\Delta(p,\omega)+4\epsilon^2\Delta(p,\omega)\times I_r(p,\omega)\times\Delta(p,\omega)\\&=\Delta(p,\omega)[1+4\epsilon^2\Delta(p,\omega)I_r(p,\omega)]\\&\Rightarrow\Delta'^{-1}(p,\omega)\\&=\Delta^{-1}(p,\omega)-4\epsilon^2 I_r(p,\omega)+O(\epsilon^4),\end{aligned}\tag{A1}$$

where the loop integral $I_r(p,\omega)$ is built up from the bare response function, the bare vertex, and the bare noise spectrum (for convenience, we have already factored the dependence on the vertex, or bare coupling ϵ, out of the loop integral). From inspection of the loop diagram and making use of the Feynman rules, this integral has a structure given by

$$\begin{aligned}I_r(p,\omega)&=\int^{>}\frac{dq}{2\pi}\int_{-\infty}^{\infty}\frac{d\Omega}{2\pi}\Delta(p-q,\omega-\Omega)C(q,\Omega)\\&=\int^{>}\frac{dq}{2\pi}\int_{-\infty}^{\infty}\frac{d\Omega}{2\pi}\frac{\Gamma(q,\Omega)}{(\Omega^2+[\nu q^2+\alpha-\beta\Omega^2]^2)[i[\omega-\Omega]-\beta[\omega-\Omega]^2+\nu(p-q)^2+\alpha]},\end{aligned}\tag{A2}$$

valid for an arbitrary Gaussian noise spectral function $\Gamma(q,\Omega)$.

The internal momentum and frequency flowing around the loop are denoted by q and Ω, respectively. The net momentum and frequency flowing into and out of the loop diagram are p and ω; note that conservation of momentum and frequency is maintained independently at each vertex. We take a white noise spectrum $\Gamma(q,\Omega)=2\mathcal{A}$, and first compute the frequency integral exactly using the residue theorem (the contour may be closed in either the upper or lower half-plane). For the one-loop corrected inverse response function [from the last line in Eq. (A1)], this yields

$$\begin{aligned}&(i\omega-\beta'\omega^2+\nu'p^2+\alpha')\\&\quad=(i\omega-\beta\omega^2+\nu p^2+\alpha)+\frac{4\epsilon^2\mathcal{A}}{\beta^2}\int^{>}\frac{dq}{2\pi}F(q;p,\omega),\end{aligned}\tag{A3}$$

where the integrand function F, which depends on both internal and external momenta as well as on the external frequency, is given by

$$\begin{aligned}F(q;p,\omega)=\frac{1}{(\Omega_1-\Omega_2)}\Bigg\{&\frac{1}{\Omega_1(\Omega_1-\Omega_3)(\Omega_1-\Omega_4)}\\&+\frac{1}{\Omega_1^*(\Omega_2-\Omega_3)(\Omega_2-\Omega_4)}\Bigg\},\end{aligned}\tag{A4}$$

and is expressed in terms of the following poles in the complex frequency plane which arise in the frequency integration:

$$\begin{aligned}\Omega_1&=\frac{1}{2\beta}(i+\sqrt{4\beta(\nu q^2+\alpha)-1}),\\\Omega_2&=\frac{1}{2\beta}(i-\sqrt{4\beta(\nu q^2+\alpha)-1}),\\\Omega_3&=\frac{1}{2\beta}(-i+\sqrt{4\beta[\nu(p-q)^2+\alpha]-1})+\omega,\\\Omega_4&=\frac{1}{2\beta}(-i-\sqrt{4\beta[\nu(p-q)^2+\alpha]-1})+\omega.\end{aligned}\tag{A5}$$

We work with the *inverse* response function since this is a simple polynomial in p and ω. To renormalize Δ^{-1}, we must expand out the momentum integral in Eq. (A3) in lowest powers in both the external frequency and momentum (ω,p), match like powers on both sides of expression (A3), and then take the hydrodynamic limits $\omega\to 0$ and $p\to 0$ at the end of the calculation. It is important to note that contributions to these asymptotic long-distance and long-time expansions come not only from Taylor-expanding the integrand F itself but also from the *domain of integration* implicit in the integral. We must integrate the loop momentum within a fixed ''shell,'' and the net momenta circulating within the loop depends on both external and internal momentum variables, and this fact must be taken into account. Thus, the resultant domain of momentum-shell integration is given by the *intersection* of the two intervals $\Lambda/s\leqslant|q|\leqslant\Lambda$ and $\Lambda/s\leqslant|p-q|\leqslant\Lambda$. Up to second order in p, the last inequality can be written as $\Lambda/s+p(|q|/q)\leqslant|q|\leqslant\Lambda+p(|q|/q)$, since the $O(p^2)$ terms vanish identically. In taking the intersection of this with the first inequality, we have four cases to consider depending on the sign of $p(p>0,p<0)$ and the sign of $|q|/q=\pm$. The resultant integration domain, valid for all four cases, can be written as the difference

$$\int^{>}\frac{dq}{2\pi}=\int_{\Lambda/s}^{\Lambda}\frac{dq}{2\pi}-\int_{\Sigma(p,s)}\frac{dq}{2\pi}, \tag{A6}$$

where the domain $\Sigma(p,s)=[\Lambda/s,\Lambda/s+p]\cup[\Lambda+p,\Lambda]\cup[\Lambda-p,\Lambda]\cup[\Lambda/s,\Lambda/s-p]$. Note of course that $\Sigma(0,s)=\Sigma(p,1)=\phi$ is just the empty set.

To proceed with the calculation, in accord with Eq. (A3), we need to expand out the function F up to and including quadratic powers in both external frequency and momentum $(1,\omega,p,p^2,\omega p,\omega^2)$, and consistently combine these with the powers of p coming from the integration over $\Sigma(p,s)$. In practice, this delicate operation need only be carried out for the renormalization of the diffusion constant ν. This is because the parameter α does not multiply any positive power of either frequency or momentum, so we can take the hydrodynamic limit at the outset in computing its one-loop correction. Next the parameter β multiplies ω^2, so we must expand the integrand F to this same order to obtain the correction β', but we can set the external momentum p to zero at the outset: the domain $\Sigma(p,s)$ does not depend on external frequency and makes no contribution to the renormalization of β. Terms linear in external frequency (ω) appearing in the loop integral do not yield any new information, since we can always redefine the time to absorb such corrections when they arise (thus we maintain the unit coefficient 1 in front of the term $i\omega$ in Δ'). Finally, for the viscosity renormalization, we can set the external frequency to zero at the outset, but must expand the integrand together with the integration domain up to and including second order in the external momentum (p). The constant contribution serves to renormalize α, as we have already remarked. Taking these points into consideration, we arrive at the following one-loop expressions for α', β',ν':

$$\alpha'=\alpha+4\frac{\epsilon^2\mathcal{A}}{\beta^2}\int_{\Lambda/s}^{\Lambda}\frac{dq}{2\pi}F(q,0,0),$$

$$\beta'=\beta-4\frac{\epsilon^2\mathcal{A}}{\beta^2}\int_{\Lambda/s}^{\Lambda}\frac{dq}{2\pi}\frac{1}{2!}\frac{\partial^2F(q,0,0)}{\partial\omega^2}, \tag{A7}$$

$$\nu' p^2=\nu p^2+4\frac{\epsilon^2\mathcal{A}}{\beta^2}\left(p^2\int_{\Lambda/s}^{\Lambda}\frac{dq}{2\pi}\frac{1}{2!}\frac{\partial^2F(q,0,0)}{\partial p^2}-p\int_{\Sigma(p,s)}\frac{dq}{2\pi}\frac{\partial F(q,0,0)}{\partial p}\right).$$

Calculating the indicated derivatives of F using the definition of Eq. (A4) together with the complex poles [Eq. (A5)] yields the following independent equations for the (one-loop) renormalized parameters, namely,

$$\alpha'=\alpha-2\epsilon^2\mathcal{A}\int_{\Lambda/s}^{\Lambda}\frac{dq}{2\pi}\frac{1}{(\nu q^2+\alpha)^2},$$

$$\beta'=\beta-\epsilon^2\mathcal{A}\int_{\Lambda/s}^{\Lambda}\frac{dq}{2\pi}\left(\frac{\beta^2}{(\nu q^2+\alpha)^2}+\frac{1}{2}\frac{1}{(\nu q^2+\alpha)^4}\right), \tag{A8}$$

$$\begin{aligned}\nu'=\nu+2\epsilon^2\mathcal{A}\int_{\Lambda/s}^{\Lambda}\frac{dq}{2\pi}&\frac{1}{[4\beta(\nu q^2+\alpha)-1]}\\&\times\left\{\left[\frac{2\nu}{\beta}-\frac{8\nu^2q^2}{4\beta(\nu q^2+\alpha)-1}\right]\left(-\frac{\beta^3}{(\nu q^2+\alpha)}\right.\right.\\&\left.+\frac{5\beta^2}{4(\nu q^2+\alpha)^2}-\frac{\beta}{4(\nu q^2+\alpha)^3}\right)\\&\left.+4\nu^2q^2\left(\frac{3\beta^2}{2(\nu q^2+\alpha)^2}-\frac{\beta}{(\nu q^2+\alpha)^3}+\frac{1}{4(\nu q^2+\alpha)^4}\right)\right\}\\&+O(\Sigma(p,s)).\end{aligned}$$

These one-loop equations are exact. We have not bothered to explicitly write out the contribution to the viscosity renormalization coming from the domain $\Sigma(p,s)$, since it is easy to show that this will vanish identically when we pass to the differential form of the renormalization group equations, i.e., in the limit of a thin shell. That is, for any function f, we have

$$\left.\frac{d}{ds}\right|_{s=1}\int_{\Sigma(p,s)}f(u)du=0. \tag{A9}$$

Applying the renormalization group procedure as described in Sec. III (a Kadanoff transformation or coarse-graining followed by a rescaling) to these equations yields the corresponding differential RG equations in (17).

APPENDIX B: NOISE SPECTRAL FUNCTION: ONE-LOOP CORRECTION

From the diagrammatic one-loop expansion for the correlation function we obtain the one-loop 1PI diagram representing the noise spectral function corrected to one-loop, as shown in the diagram in Fig. 4. This translates into the fol-

lowing mathematical equation (after factoring out the dependence on the bare vertex or coupling) for a general Gaussian noise spectral function:

$$\Gamma'(p,\omega)=\Gamma(p,\omega)+2\epsilon^2 I_n(p,\omega), \tag{B1}$$

which, for the case of white noise considered here, reduces to

$$2\mathcal{A}'=2\mathcal{A}+2\epsilon^2 I_n(p,\omega). \tag{B2}$$

The loop integral I_n depends in general on external frequency and momentum, whose structure is given by

$$I_n(p,\omega)=\int^{>}\frac{dq}{2\pi}\int_{-\infty}^{\infty}\frac{d\Omega}{2\pi}C(q,\omega)C(p-q,\Omega-\omega), \tag{B3}$$

but since the noise spectrum is constant, we can take the hydrodynamic limit right away and evaluate the somewhat simpler integral

$$I_n(0,0)=\int_{\Lambda/s}^{\Lambda}\frac{dq}{2\pi}\int_{-\infty}^{\infty}\frac{d\Omega}{2\pi}\frac{4\mathcal{A}^2}{[\Omega^2+(\nu q^2-\beta\Omega^2+\alpha)^2]^2}. \tag{B4}$$

Once again, the frequency integration can be evaluated easily by the method of residues. Doing so, we obtain the one-loop correction to the white noise amplitude

$$\mathcal{A}'=\mathcal{A}+4\epsilon^2\mathcal{A}^2\int_{\Lambda/s}^{\Lambda}\frac{dq}{2\pi}\frac{1}{4\beta(\nu q^2+\alpha)-1}\times\left(\frac{\beta^2}{(\nu q^2+\alpha)}+\frac{3}{4}\frac{\beta}{(\nu q^2+\alpha)^2}-\frac{1}{4(\nu q^2+\alpha)^3}\right). \tag{B5}$$

Applying the renormalization group procedure to this equation yields the corresponding RG equation for the noise amplitude given in Eq. (17).

APPENDIX C: VERTEX FUNCTION: ONE-LOOP CORRECTION

The diagrammatic expansion for the one-loop correction to the vertex function, or coupling constant, is depicted as shown in Fig. 3. For general vertex functions, momentum and frequency (i.e., energy) conservation implies that a trilinear vertex can depend on at most two independent external momenta and two independent external frequencies. Which two momenta and which two frequencies one chooses is immaterial. Translating the vertex diagrams into corresponding mathematical elements for the one-loop vertex correction yields the equation.

$$\epsilon'=\epsilon+4\epsilon^3 I_v(k_1,\omega_1;k_2,\omega_2). \tag{C1}$$

The structure of the one-loop integral is given as follows:

$$\begin{aligned}I_v(k_1,\omega_1;k_2,\omega_2)&=\int^{>}\frac{dq}{2\pi}\int_{-\infty}^{\infty}\frac{d\Omega}{2\pi}\{C(q,\Omega)\Delta(q-k_2,\Omega-\omega_2)\\&\times\Delta(q-k_1,\Omega-\omega_1)+\Delta(-q,-\Omega)\\&\times C(q-k_2,\Omega-\omega_2)\Delta(q-k_1,\Omega-\omega_1)\\&+\Delta(-q,-\Omega)\Delta(k_2-q,\omega_2-\Omega)C(k_1-q,\omega_1-\Omega)\}.\end{aligned} \tag{C2}$$

However, since the coupling ϵ is constant, in anticipation of the hydrodynamic limit we can immediately set all external momenta and frequencies to zero in computing the one-loop correction to ϵ. Taking this limit, and taking a white noise spectral function, we have that the vertex loop integral at zero external momentum and frequency is given by

$$\begin{aligned}I_v(0,0;0,0)&=\int^{>}\frac{dq}{2\pi}\int_{-\infty}^{\infty}\frac{d\Omega}{2\pi}\frac{2\mathcal{A}}{[\Omega^2+(\nu q^2-\beta\Omega^2+\alpha)^2]}\\&\times\left(\frac{1}{(i\Omega-\beta\Omega^2+\nu q^2+\alpha)^2}\right.\\&+\frac{1}{(i\Omega-\beta\Omega^2+\nu q^2+\alpha)(-i\Omega-\beta\Omega^2+\nu q^2+\alpha)}\\&\left.+\frac{1}{(-i\Omega-\beta\Omega^2+\nu q^2+\alpha)^2}\right).\end{aligned} \tag{C3}$$

The integral over the internal frequency may be performed exactly, once again by the method of residues. This yields

$$\begin{aligned}\epsilon'=\epsilon+8\epsilon^3\mathcal{A}\int_{\Lambda/s}^{\Lambda}\frac{dq}{2\pi}&\left(\frac{1}{4(\nu q^2+\alpha)^3}-\frac{\beta}{4(\nu q^2+\alpha)^2}\right.\\&+\frac{1}{(4\beta(\nu q^2+\alpha)-1)}\left\{\frac{\beta^2}{(\nu q^2+\alpha)}+\frac{3\beta}{4(\nu q^2+\alpha)^2}\right.\\&\left.\left.-\frac{1}{4(\nu q^2+\alpha)^3}\right\}\right).\end{aligned} \tag{C4}$$

Applying the renormalization group procedure to this equation yields the differential RG equation for the coupling listed in Eq. (17).

APPENDIX D: CORRELATED NOISE

The effect of both temporal and/or spatial correlations in the Gaussian noise spectrum can be also be taken into account in this model. Here, we briefly indicate what steps would have to be taken or modified in the renormalization group program to include such correlations. In Eq. (2) the spectral function with both uncorrelated (white) and correlated (colored) components is written

$$\Gamma(k,\omega)=2\mathcal{A}+2\mathcal{A}_{\rho,\theta}\left(\frac{k^2}{\Lambda^2}\right)^{-\rho}\left(\frac{\omega^2}{\omega_0^2}\right)^{-\theta}, \tag{D1}$$

where we consider long-range correlations of the power-law type. These are parametrized in terms of two exponents ρ and θ for spatially and temporally correlated noise, respectively. The naive scaling properties [Eq. (5)] of the stochastic

equation are extended to include the scaling of the correlated part of the noise, which reads

$$\mathcal{A}_{\rho,\theta} \to s^{2\rho-1-2\chi+z(2\theta+1)} \mathcal{A}_{\rho,\theta}. \tag{D2}$$

The perturbative expansion for the response, noise and vertex goes through as before, except now, for $\theta \neq 0$, the one-loop frequency integrations over Ω must be recalculated and, in general, branch cuts and poles must be dealt with in the complex Ω plane. The RG equations will now depend on the two noise exponents ρ and θ, as will the fixed points and the critical exponents: $z = z(\rho, \theta)$, and $\chi = \chi(\rho, \theta)$. There will be an additional RG equation for the amplitude of the colored component of the noise yielding a total of six equations. By Buckingham's Π theorem [30], we know that these can be cast in terms of four equations in four dimensionless variables. In effect, the correlations in the noise ''open up'' a new direction in parameter space, and yield a correspondingly more complicated fixed point and RG flow structure than that of the uncorrelated noise case treated here.

[1] S.-K. Ma, Modern *Theory of Critical Phenomena* (Addison-Wesley, Reading, MA, 1976).
[2] J. Cardy, *Scaling and Renormalization in Statistical Physics* (Cambridge University Press, Cambridge, England, 1996).
[3] D. Forster, D. R. Nelson, and M. J. Stephen, Phys. Rev. A **16**, 732 (1977).
[4] V. Yakhot and S. A. Orszag, Phys. Rev. Lett. **57**, 1722 (1986).
[5] U. Frisch, *Turbulence* (Cambridge University Press, Cambridge, England, 1995).
[6] M. Kardar, G. Parisi, and Y.-C. Zhang, Phys. Rev. Lett. **56**, 889 (1986).
[7] E. Medina, T. Hwa, M. Kardar, and Y.-C. Zhang, Phys. Rev. A **39**, 3053 (1989).
[8] T. Sun and M. Plischke, Phys. Rev. E **49**, 5046 (1994).
[9] E. Frey and U. C. Tauber, Phys. Rev. E **50**, 1024 (1994).
[10] A.-L. Barabási and H. E. Stanley, *Fractal Concepts in Surface Growth* (Cambridge University Press, Cambridge, England, 1995).
[11] R. Cuerno and K. B. Lauritsen, preprint cond-mat/9505076.
[12] A. Berera and L.-Z. Fang, Phys. Rev. Lett. **72**, 458 (1994).
[13] D. Hochberg and J. Pérez-Mercader, Gen. Relativ. Gravit. **28**, 1427 (1996).
[14] T. Goldman, D. Hochberg, R. Laflamme, and J. Pérez-Mercader, Phys. Lett. A **222**, 177 (1996).
[15] J. F. Barbero, A. Domínguez, T. Goldman, and J. Pérez-Mercader, Europhys. Lett. **38**, 637 (1997).
[16] A. Domínguez, D. Hochberg, J. M. Martín-García, J. Pérez-Mercader, and L. S. Schulman, Astron. Astrophys. **344**, 27 (1999).
[17] C. C. Chow and J. J. Collins, Phys. Rev. E **52**, 907 (1995).
[18] J. J. Collins and C. J. DeLuca, Phys. Rev. Lett. **73**, 764 (1994).
[19] M. Lauk, C. C. Chow, A. E. Pavlik and J. J. Collins, Phys. Rev. Lett. **80**, 413 (1998).
[20] G. McCollum and T. K. Leen, J. Motor Behav. **21**, 225 (1985).
[21] L. M. Nasher (unpublished).
[22] D. Hochberg, C. Molina-París, J. Perez-Mercader, and M. Visser, Phys. Rev. E **60**, 6343 (1999).
[23] J. Zinn-Justin, *Quantum Field Theory and Critical Phenomena* (Oxford University Press, Oxford, 1996).
[24] R. J. Rivers, *Path Integral Methods in Quantum Field Theory* (Cambridge University Press, Cambridge, England, 1987).
[25] S. F. Edwards and D. R. Wilkinson, Proc. R. Soc. London, Ser. A **381**, 17 (1982).
[26] P. C. Martin, E. D. Siggia, and H. A. Rose, Phys. Rev. A **8**, 423 (1973).
[27] C. De Dominicis and L. Peliti, Phys. Rev. B **18**, 353 (1978).
[28] H. K. Janssen, Z. Phys. B: Condens. Matter Quanta **23**, 377 (1976); R. Bausch, H. K. Janssen, and H. Wagner, *ibid.* **24**, 113 (1976).
[29] D. Amit, *Field Theory, the Renormalization Group, and Critical Phenomena* (McGraw-Hill, New York, 1978).
[30] E. Buckingham, Phys. Rev. **4**, 345 (1914).
[31] R. K. Koleva, A. Widom, D. Garelik, and M. Harris, e-print cond-mat/9907311.
[32] V. Konotop and L. Vázquez, *Nonlinear Random Waves* (World Scientific, Singapore, 1994).